12^{th} International Conference on Fracture Mechanics of Concrete and Concrete Structures
FraMCoS-12
B.L.A. Pichler, Ch. Hellmich, P. Preinstorfer (Eds)

https://doi.org/10.21012/FC12.1263
MS10-1:1

ASYMPTOTIC HOMOGENIZATION OF DISCRETE MODELS WITH ROTATIONAL DEGREES OF FREEDOM

JAN ELIÁŠ*, GIANLUCA CUSATIS†

* Brno University of Technology, Faculty of Civil Engineering, Institute of Structural Mechanics
Veveří 331/95, Brno, 60200
e-mail: jan.elias@vut.cz

†Northwestern University, Department of Civil and Environmental Engineering
2145 Sheridan Road, Evanston, IL 60208, USA
e-mail: g-cusatis@northwestern.edu

Key words: Discrete model, Lattice, Homogenization, Rotation, Cauchy-Continuum

Abstract. This contribution revisits the homogenization techniques applied to discrete models incorporating rotational degrees of freedom. The theoretical framework extends previous work on the homogenization of Cosserat continua, demonstrating how these models can be homogenized to a Cauchy continuum under realistic assumptions. The formulation is developed within the context of linear elasticity and validated through simulations of a bent cantilever.

1 INTRODUCTION

Heterogeneous materials such as concrete are critical in civil engineering. Their mechanical behavior is therefore subject of long lasting research. The ability to simulate these materials on a large, structural scale while reflecting its heterogeneous mesoscale character is founded on homogenization techniques. The classical asymptotic expansion homogenization developed by Sanchez-Palencia [15, 16] and others is used here do derive macroscopic behavior of elastic discrete mesoscale models of concrete.

The discrete models with fixed underlying lattice structure are extremely powerful numerical tools for simulating concrete inelastic behavior, including tensile, compressive and triaxial loading scenarios [4]. Part of this success lies in vectorial constitutive equations that are oriented and simpler to develop compare to tensorial, frame invariant approaches. Another part lies in heterogeneous nature of models with *physical* discretization. There is a large number of such models available including the original lattice models [18, 17], mechanical particle-based models [12, 5, 2] and coupled multiphysical models [11, 10, 19]. In this work we follow the line of mechanical particle models arising from Voronoi and power tessellation as proposed by Bolander and Saito [3].

Homogenization of these discrete structures was already developed in Refs. [13, 14, 7]. The resulting macroscale emerging from homogenization was Cosserat continuum. In the present contribution, the work of Forest, Pradel, and Sab [9] on continuous Cosserat models is followed, the resulting continuum turns to be of Cauchy type. In practice, all the previous results are identical to the new one as the previously acknowledged macroscopic Cosserat effects are typically negligible.

2 DISCRETE MODEL EQUATION

The domain is filed with spherical aggregates generated according to Fuller's curve and

power tessellation is performed. The cells I of the tessellation are treated as ideally rigid bodies with the governing node $\mathbf{x}_I$ bearing three displacements $\mathbf{u}_I$ and three rotations $\boldsymbol{\theta}_I$.

The kinematic equation provides strain between particle I and J in local orthonormal coordinate system $\mathbf{n}_\alpha$, $\alpha \in (N, M, L)$, with N being the normal direction and M and L the tangential directions

$$e_\alpha^{IJ} = \frac{1}{l}\left[\mathbf{u}_J - \mathbf{u}_I + \boldsymbol{\mathcal{E}} : (\boldsymbol{\theta}_J \otimes \mathbf{c}_J - \boldsymbol{\theta}_I \otimes \mathbf{c}_I)\right] \cdot \mathbf{n}_\alpha^{IJ} \tag{1}$$

$\mathbf{c}$ is a vector connecting particle governing node (I or J) with the integration point $\mathbf{x}_c$ at the contact face, $\boldsymbol{\mathcal{E}}$ is Levi-Civita permutation tensor. The contact length $l = ||\mathbf{x}_J - \mathbf{x}_I||$ and the contact normal $\mathbf{n}_N = (\mathbf{x}_J - \mathbf{x}_I)/l$. The last expression is ensured by the power tessellation that always creates facets perpendicular to the branch vectors.

The constitutive equation relates strain to the traction vector, $\mathbf{t}$. Considering the linear elasticity and the standard form used in discrete modeling, the traction reads

$$t_N^{IJ} = E_0 e_N^{IJ} \tag{2a}$$
$$t_M^{IJ} = E_0 \alpha e_M^{IJ} \tag{2b}$$
$$t_L^{IJ} = E_0 \alpha e_L^{IJ} \tag{2c}$$

with E_0 and α being two independent material elastic parameters.

The balances of linear and angular momentum in steady state for each particle read

$$-V_I \mathbf{b} = \sum_J A_{IJ} t_\alpha^{IJ} \mathbf{n}_\alpha^{IJ} \tag{3a}$$
$$-V_I \mathbf{z} = \sum_J A_{IJ} t_\alpha^{IJ} \boldsymbol{\mathcal{E}} : (\mathbf{c}_I \otimes \mathbf{n}_\alpha^{IJ}) \tag{3b}$$

where J runs over all neighbors of particle I and $\mathbf{b}$ and $\mathbf{z}$ are external volume force and volume couple. Boundary conditions prescribe either values of the degrees of freedom or associated reaction forces or couples.

3 SCALE SEPARATION

The periodic Representative Volume Element of characteristic size l_c is considered as a building block of the whole model of characteristic size L_c. The unique macroscopic reference system is denoted $\mathbf{X}$, its dimensionless version is $\tilde{\mathbf{X}} = \mathbf{X}/L_c$. At each macroscale point the RVE reference systems $\mathbf{y}$ is defined with dimensionless version $\tilde{\mathbf{y}} = \mathbf{y}/l_c$. A positive scale separation constant then reads $\eta = l_c/L_c$.

A limit situation when η approaches zero is studied. According to Refs. [1, 16] each dimensionless model variable $\tilde{\bullet}$ can be written in an expanded form as a series of periodic functions of two independent dimensionless spatial coordinates $\tilde{\mathbf{X}}$ and $\tilde{\mathbf{y}}$

$$\tilde{\bullet}(\tilde{\mathbf{X}}, \tilde{\mathbf{y}}) = \tilde{\bullet}^{(0)}(\tilde{\mathbf{X}}, \tilde{\mathbf{y}}) + \eta \tilde{\bullet}^{(1)}(\tilde{\mathbf{X}}, \tilde{\mathbf{y}}) + \dots \tag{4}$$

The dimensionless displacements $\tilde{\mathbf{u}} = \mathbf{u}/u_c$ and rotations $\tilde{\boldsymbol{\theta}} = \boldsymbol{\theta}/\theta_c$ are considered in the expanded form. However, the rotations are first re-written as a combination of the dependent and independent components

$$\tilde{\boldsymbol{\theta}} = \tilde{\boldsymbol{\omega}} + \tilde{\boldsymbol{\varphi}} \tag{5}$$

$\boldsymbol{\omega}$ is the dependent part dictated by the curl of the displacement field. The expansion is applied only to the independent part, $\tilde{\boldsymbol{\varphi}}$

$$\tilde{\mathbf{u}}(\tilde{\mathbf{X}}, \tilde{\mathbf{y}}) = \tilde{\mathbf{u}}^{(0)}(\tilde{\mathbf{X}}, \tilde{\mathbf{y}}) + \eta \tilde{\mathbf{u}}^{(1)}(\tilde{\mathbf{X}}, \tilde{\mathbf{y}}) + \dots \tag{6a}$$

$$\tilde{\boldsymbol{\varphi}}(\tilde{\mathbf{X}}, \tilde{\mathbf{y}}) = \tilde{\boldsymbol{\varphi}}^{(0)}(\tilde{\mathbf{X}}, \tilde{\mathbf{y}}) + \eta \tilde{\boldsymbol{\varphi}}^{(1)}(\tilde{\mathbf{X}}, \tilde{\mathbf{y}}) + + \dots \tag{6b}$$

According to Fish, Chen, and Li [8] the Taylor series approximates the mechanical field variables at node J based on information at the neighboring node I

$$\tilde{\mathbf{u}}(\tilde{\mathbf{X}}_J, \tilde{\mathbf{y}}_J) = \tilde{\mathbf{u}}(\tilde{\mathbf{X}}_I, \tilde{\mathbf{y}}_J) + \eta \frac{\partial \tilde{\mathbf{u}}(\tilde{\mathbf{X}}_I, \tilde{\mathbf{y}}_J)}{\partial \tilde{X}_j} \tilde{x}_j^{IJ} + \dots \tag{7a}$$

$$\tilde{\boldsymbol{\varphi}}(\tilde{\mathbf{X}}_J, \tilde{\mathbf{y}}_J) = \tilde{\boldsymbol{\varphi}}(\tilde{\mathbf{X}}_I, \tilde{\mathbf{y}}_J) + \eta \frac{\partial \tilde{\boldsymbol{\varphi}}(\tilde{\mathbf{X}}_I, \tilde{\mathbf{y}}_J)}{\partial \tilde{X}_j} \tilde{x}_j^{IJ} + \dots \tag{7b}$$

The dependent part of the rotation is expressed as the half of the curl of the displacement

field with nabla ∇ operator considered according to the chain rule $\nabla \rightarrow \nabla_X + \nabla_y = 1/l_c\,(\eta\nabla_{\tilde{X}} + \nabla_{\tilde{y}})$.

$$\tilde{\boldsymbol{\omega}} = \frac{1}{2}\boldsymbol{\mathcal{E}} : (\eta\nabla_{\tilde{X}} \otimes \tilde{\mathbf{u}} + \nabla_{\tilde{y}} \otimes \tilde{\mathbf{u}}) \tag{8}$$

where the displacement field in the expanded form shall be inserted.

The relative magnitude of the normalization parameters u_c, θ_c, ω_c, and φ_c is considered in the following way: $\theta_c \sim \omega_c \sim \varphi_c \sim u_c/l_c$. Combining the expansions (6) with Eq. (7) and Eq. (1) the asymptotic expansion of strain is obtained. The constitutive model maps the strain to the traction, $\mathbf{t}$, which reads in the expanded form

$$\tilde{\mathbf{t}} = \tilde{\mathbf{t}}^{(0)} + \eta\tilde{\mathbf{t}}^{(1)} + \dots \tag{9}$$

where the terms $\mathbf{t}^{(i)}$ can be easily derived directly from the equations above. The normalization constant for traction is $t_c = E_c u_c/l_c$.

The balance equations then yields

$$-l_c^3 b_c \tilde{V}\tilde{\mathbf{b}} = l_c^2 t_c \sum_J \tilde{A}\tilde{t}_\alpha \mathbf{n}_\alpha \tag{10a}$$

$$-l_c^3 z_c \tilde{V}\tilde{\mathbf{z}} = l_c^2 \sum_J A l_c t_c \tilde{t}_\alpha \boldsymbol{\mathcal{E}} : (\tilde{\mathbf{c}}_I \otimes \mathbf{n}_\alpha) \tag{10b}$$

where volume and area are scaled as $V = l_c^3\tilde{V}$ and $A = l_c^2\tilde{A}$ since they are dictated by particle size comparable to the RVE size, l_c. It is reasonable to assume that volume force and couple act at the macroscale. This is achieved by assuming $b_c \sim E_c u_c/L_c^2$ and $z_c \sim E_c u_c/L_c$. The balance equations in their dimensionless form then read

$$-\eta^2\tilde{V}\tilde{\mathbf{b}} = \sum_J \tilde{A}\tilde{t}_\alpha \mathbf{n}_\alpha \tag{11a}$$

$$-\eta\tilde{V}\tilde{\mathbf{z}} = \sum_J \tilde{A}\tilde{t}_\alpha \boldsymbol{\mathcal{E}} : (\tilde{\mathbf{c}}_I \otimes \mathbf{n}_\alpha) \tag{11b}$$

These equations are now written at appropriate levels – powers of η. They are also brought back to the original dimensional format. The linear momentum balances yield

$$\eta^0 : \qquad \mathbf{0} = \sum_J A t_\alpha^{(0)} \mathbf{n}_\alpha \tag{12a}$$

$$\eta^1 : \qquad \mathbf{0} = \sum_J A\eta t_\alpha^{(1)} \mathbf{n}_\alpha \tag{12b}$$

$$\eta^2 : \qquad -V\mathbf{b} = \sum_J A\eta^2 t_\alpha^{(2)} \mathbf{n}_\alpha \tag{12c}$$

while the angular momentum balance read

$$\eta^0 : \qquad \mathbf{0} = \sum_J A t_\alpha^{(0)} \boldsymbol{\mathcal{E}} : (\mathbf{c}_I \otimes \mathbf{n}_\alpha) \tag{13a}$$

$$\eta^1 : \quad -V\mathbf{z} = \sum_J A\eta t_\alpha^{(1)} \boldsymbol{\mathcal{E}} : (\mathbf{c}_I \otimes \mathbf{n}_\alpha) \tag{13b}$$

Balance equations at the higher scales are not entering the the first order solution and are therefore omitted.

These equations are now solved sequentially. At scale η^0 the degrees of freedom are $\mathbf{u}^{(0)}$ and $\boldsymbol{\varphi}^{(0)}$ and the solution reads

$$\mathbf{u}^{(0)} = \text{constant in } y \qquad \boldsymbol{\varphi}^{(0)} = \mathbf{0} \tag{14}$$

At the next scale with with degrees of freedom $\eta\mathbf{u}^{(1)}$ and $\eta\boldsymbol{\varphi}^{(1)}$ the solution must be solved numerically. The degrees of freedom for the submodel are in the following form

$$\mathbf{u}^{\text{mic}} = \eta\mathbf{u}^{(1)} \tag{15a}$$

$$\boldsymbol{\theta}^{\text{mic}} = \eta\boldsymbol{\varphi}^{(1)} + \frac{\eta}{2}\boldsymbol{\mathcal{E}} : \nabla_y \otimes \mathbf{u}^{(1)} \tag{15b}$$

These variables are found using RVE with periodic boundary conditions, loading is provided by projecting macroscopic strain tensor onto the elements as eigenstrain. The kinematic, constitutive and balance equations to be solved are exactly those from Sec. 2 providing the particle displacements and rotations are $\mathbf{u}^{\text{mic}}$ and $\boldsymbol{\theta}^{\text{mic}}$.

The last step ensures the overall balance of the whole RVE. The balance equations (12) and (13) are therefore summed over the RVE. The first meaningful equations, after some mathematical modifications, lead to the definition of macroscopic stress

$$\boldsymbol{\sigma}^{\text{mac}} = \frac{1}{V_0}\sum_{e\in V_0} l A\eta t_\alpha^{(1)} \mathbf{n}_N \otimes \mathbf{n}_\alpha \tag{16}$$

and macroscale balance equations

$$-\langle \mathbf{b} \rangle = \nabla_X \cdot \boldsymbol{\sigma}^{\mathrm{mac}} \tag{17a}$$

$$-\langle \mathbf{z} \rangle = \boldsymbol{\mathcal{E}} : \boldsymbol{\sigma}^{\mathrm{mac}} \tag{17b}$$

where $\langle \bullet \rangle$ is the volumetric average of variable $\bullet$ over the RVE. The first equation is the standard balance equation of Cauchy continuum for unknown macroscopic displacement $\mathbf{u}^{(0)}$ while the second equation dictates symmetry of the stress tensor.

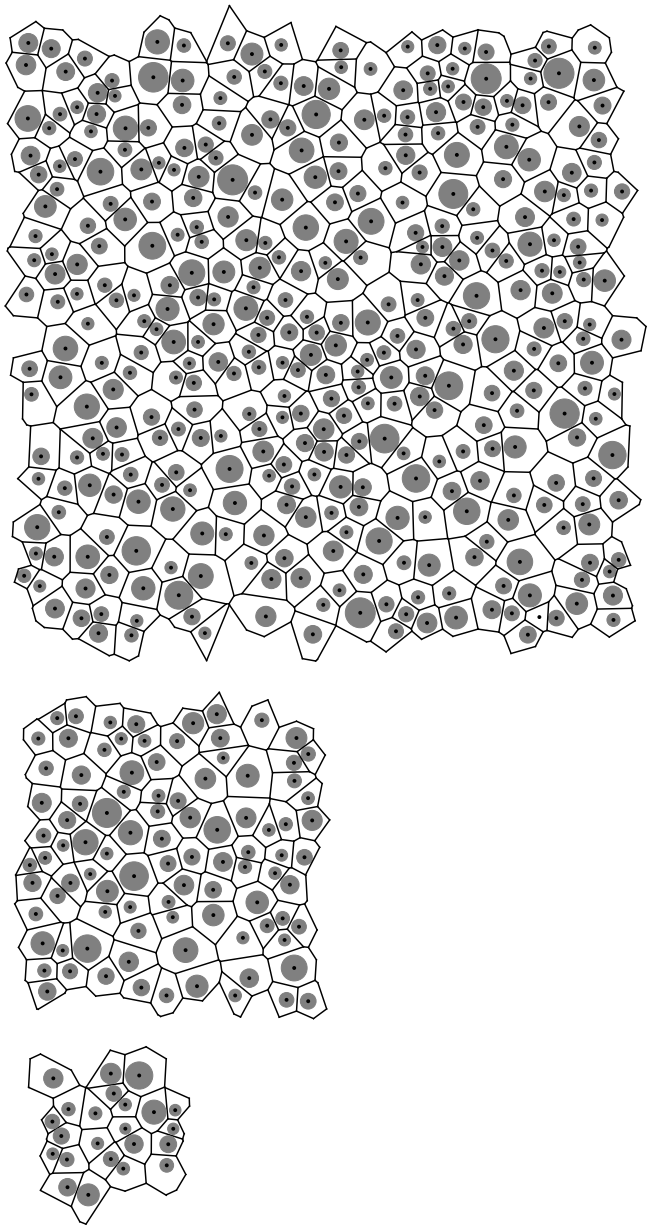

Figure 1: Examples of periodic discrete structures used to compute homogenized response at the RVE scale: from the bottom $l_c = 0.05$, 0.1, and 0.2 m.

4 VERIFICATION

Two dimensional model of a cantilever of size $1\times6\,\mathrm{m}^2$ is loaded by force at the end. The *homogenized* model meshes the cantilever by square bilinear isoparametric Cauchy finite elements of size $0.025\times0.025\,\mathrm{m}^2$, there is therefore 40×240 such elements. Each integration point contains a precomputed square periodic RVE submodel of sizes $l_c = 0.05$, 0.1 and 0.2 m. RVEs are represented by discrete models created by randomly placing circular aggregates with no overlapping and subsequently performing the power tesselation. Aggregate diameters are given by Fuller curve, the maximum diameter is 10 mm and the minimum one considered is 4 mm, see Fig. 1. The same discrete model is used as the *full* model for the whole cantilever. Bending stiffness (loading force causing unit deflection) is computed for all *homogenized* and *full* models.

The discrete model response is essentially random due to random location of the aggregates. To reduce this randomness, there are 6 *full* models and 50 *homogenized* models for each RVE size used to obtain statistical characteristics of the bending stiffness. The average and standard deviation of the stiffness is shown in Fig. 2.

The bending stiffness mean value of the *full* and *homogenized* models is almost identical. The difference shall be attributed to (i) insufficient statistical sample size and also (ii) some small differences in the structure of the discrete model due to boundary layer effect present in the *full* model [6]. The maximum difference is about then 0.5 %. The standard deviation of the *full* model is quite low compared to the *homogenized* models thanks to the large number of particles. As the RVE size increases, the standard deviation of the *homogenized* models decreases due to the same reason.

5 CONCLUSIONS

Following the work of Forest, Pradel, and Sab [9], the discrete model with rotational degrees of freedom is homogenized into Cauchy continuum. The angular momentum balance

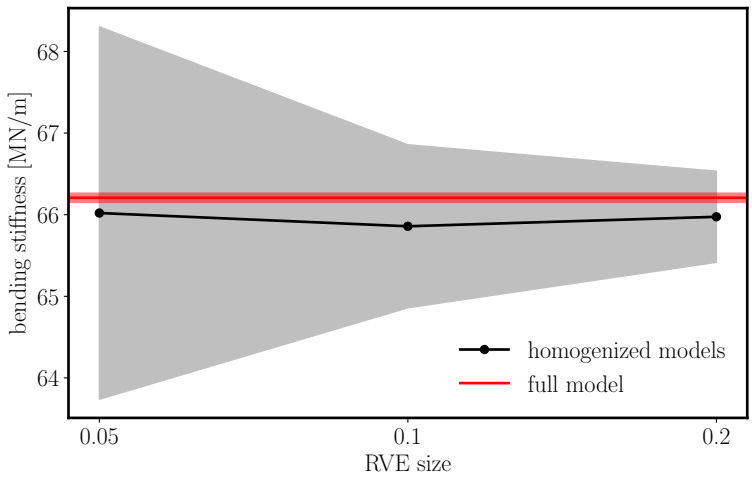

Figure 2: Bending stiffness of the cantilever computed by the full models and homogenized models of different RVE size.

equation ensures the stress tensor symmetry. To derive this result, rotations of the particles must be decomposed into the part dependent on curl of the displacement field and the independent part. Simple verification example confirmed the derived equations.

ACKNOWLEDGEMENT

Jan Eliáš gratefully acknowledges financial support from the Czech Science Foundation under project number GA24-11845S. Gianluca Cusatis acknowledges support by the Engineering Research and Development Center (ERDC) – Construction Engineering Research Laboratory (CERL) under Contract No. W9132T22C0015.

References

[1] A. Bensoussan, J.-L. Lions, and G. Papanicolaou. *Asymptotic Analysis for Periodic Structures*. North-Holland, 1978.

[2] Tathagata Bhaduri, Shady Gomaa, and Mohammed Alnaggar. "Coupled Experimental and Computational Investigation of the Interplay between Discrete and Continuous Reinforcement in Ultrahigh Performance Concrete Beams. II: Mesoscale Modeling". In: *Journal of Engineering Mechanics* 147.9 (2021), p. 04021050. DOI: 10.1061/(ASCE)EM.1943-7889.0001941.

[3] J.E. Bolander and S. Saito. "Fracture analyses using spring networks with random geometry". In: *Engineering Fracture Mechanics* 61.5 (1998), pp. 569–591. ISSN: 0013-7944. DOI: 10.1016/S0013-7944(98)00069-1.

[4] John E. Bolander et al. "Discrete mechanical models of concrete fracture". In: *Engineering Fracture Mechanics* 257 (2021), p. 108030. ISSN: 0013-7944. DOI: 10.1016/j.engfracmech.2021.108030.

[5] Gianluca Cusatis, Daniele Pelessone, and Andrea Mencarelli. "Lattice Discrete Particle Model (LDPM) for failure behavior of concrete. I: Theory". In: *Cement and Concrete Composites* 33.9 (2011), pp. 881–890. ISSN: 0958-9465. DOI: 10.1016/j.cemconcomp.2011.02.011.

[6] Jan Eliáš. "Boundary Layer Effect on Behavior of Discrete Models". In: *Materials* 10 (2017), p. 157. ISSN: 1996-1944. DOI: 10.3390/ma10020157.

[7] Jan Eliáš and Gianluca Cusatis. "Homogenization of discrete mesoscale model of concrete for coupled mass transport and mechanics by asymptotic expansion". In: *Journal of the Mechanics and Physics of Solids* 167 (2022), p. 105010. ISSN: 0022-5096. DOI: 10.1016/j.jmps.2022.105010.

[8] Jacob Fish, Wen Chen, and Renge Li. "Generalized mathematical homogenization of atomistic media at finite temperatures in three dimensions". In: *Computer Methods in Applied Mechanics and Engineering* 196.4 (2007), pp. 908–922. ISSN: 0045-7825. DOI: 10.1016/j.cma.2006.08.001.

[9] Samuel Forest, Francis Pradel, and Karam Sab. "Asymptotic analysis of heterogeneous Cosserat media". In: *International Journal of Solids and Structures* 38.26 (2001), pp. 4585–4608. ISSN: 0020-7683. DOI: 10.1016/S0020-7683(00)00295-X.

[10] Jan Mašek, Josef Květoň, and Jan Eliáš. "Adaptive discretization refinement for discrete models of coupled mechanics and mass transport in concrete". In: *Construction and Building Materials* 395 (2023), p. 132243. ISSN: 0950-0618. DOI: 10.1016/j.conbuildmat.2023.132243.

[11] Taito Miura, Hikaru Nakamura, and Yoshihito Yamamoto. "Expansive spalling mechanism of concrete due to high temperature based on developed hygro-thermal-mechanical model by 3D-RBSM-TNM". In: *Engineering Fracture Mechanics* 284 (2023), p. 109216. ISSN: 0013-7944. DOI: 10.1016/j.engfracmech.2023.109216.

[12] Kohei Nagai, Y. Sato, and Tamon Ueda. "Mesoscopic simulation of failure of mortar and concrete by 3D RBSM". In: *Journal of Advanced Concrete Technology* 3.3 (2005), pp. 385–402.

[13] Roozbeh Rezakhani and Gianluca Cusatis. "Asymptotic expansion homogenization of discrete fine-scale models with rotational degrees of freedom for the simulation of quasi-brittle materials". In: *Journal of the Mechanics and Physics of Solids* 88 (2016), pp. 320–345. ISSN: 0022-5096. DOI: 10.1016/j.jmps.2016.01.001.

[14] Roozbeh Rezakhani, Xinwei Zhou, and Gianluca Cusatis. "Adaptive multiscale homogenization of the lattice discrete particle model for the analysis of damage and fracture in concrete". In: *International Journal of Solids and Structures* 125 (2017), pp. 50–67. ISSN: 0020-7683. DOI: h10.1016/j.ijsolstr.2017.07.016.

[15] Enrique Sanchez-Palencia. "Comportements local et macroscopique d'un type de milieux physiques heterogenes". In: *International Journal of Engineering Science* 12.4 (1974), pp. 331–351. ISSN: 0020-7225. DOI: 10.1016/0020-7225(74)90062-7.

[16] Enrique Sanchez-Palencia. *Non-Homogeneous Media and Vibration Theory*. Lectures notes in Physics. Germany; New York, NY, USA, 1980.

[17] E. Schlangen and E.J. Garboczi. "Fracture simulations of concrete using lattice models: Computational aspects". In: *Engineering Fracture Mechanics* 57.2 (1997), pp. 319–332. ISSN: 0013-7944. DOI: 10.1016/S0013-7944(97)00010-6.

[18] E. Schlangen and J.G.M. van Mier. "Simple lattice model for numerical simulation of fracture of concrete materials and structures". In: *Materials and Structures* 25 (1992), pp. 534–542. ISSN: 1359–5997. DOI: 10.1007/BF02472449.

[19] Hao Yin et al. "An interprocess communication-based two-way coupling approach for implicit–explicit multiphysics lattice discrete particle model simulations". In: *Engineering Fracture Mechanics* 310 (2024), p. 110515. ISSN: 0013-7944. DOI: 10.1016/j.engfracmech.2024.110515.